photonics

MDPI

Article

Nonlinear Optical Response of Dispersed Medium Based on Conjugates Single-Walled Carbon Nanotubes with Phthalocyanines

Pavel N. Vasilevsky [1,2], Mikhail S. Savelyev [1,3], Alexander Yu. Tolbin [4], Artem V. Kuksin [1,2], Yulia O. Vasilevskaya [2,5], Andrey P. Orlov [2,6], Yury P. Shaman [2,5], Alexander A. Dudin [2], Alexander A. Pavlov [2] and Alexander Yu. Gerasimenko [1,3,*]

1 Institute of Biomedical Systems, National Research University of Electronic Technology, 124498 Zelenograd, Russia; pavelvasilevs@yandex.ru (P.N.V.)
2 Institute of Nanotechnology of Microelectronics of the Russian Academy of Sciences, 119991 Moscow, Russia
3 Institute for Bionic Technologies and Engineering, I. M. Sechenov First Moscow State Medical University, 119991 Moscow, Russia
4 Institute of Physiologically Active Compounds at Federal Research Center of Problems of Chemical Physics and Medicinal Chemistry, Russian Academy of Sciences, 142432 Chernogolovka, Russia
5 Scientific-Manufacturing Complex "Technological Centre", 124498 Moscow, Russia
6 The Kotel'nikov Institute of Radio Engineering and Electronics of the Russian Academy of Sciences, 125009 Moscow, Russia
* Correspondence: gerasimenko@bms.zone

Abstract: Nanosecond lasers have recently been widely involved in human activity. However, high-intensity laser radiation can cause severe damage to organs of vision and expensive photonic devices. Radiation in the near UV range is especially dangerous for human eyes, since it is strongly absorbed by biological media and is also invisible, i.e., the reaction time of the eye to such radiation is much lower than that of visible light. Passive limiters have high transmission (>70%) at a low light intensity and begin to "darken" only when the threshold value of the laser radiation intensity is reached. In this work, we studied liquid nanodispersed nonlinear optical limiters based on hybrids of single-walled carbon nanotubes (SWCNTs) with metal-free tetra(hydroxy)phthalocyanine $(OH)_4$PcHH). The value of the hydrodynamic radius of separate particles after $(OH)_4$PcHH binding increased from 288 ± 55 nm to 350 ± 60 nm, which confirms the attachment of phthalocyanine complexes to nanotubes. The third harmonic of a Nd:YAG nanosecond laser (355 nm, 20 ns) was used to study the nonlinear optical response. Based on a Z-scan with open-aperture and input-output dependence curves, third-order nonlinear optical absorption coefficients of 149, 236, and 229 cm/GW were obtained for dispersions of composites of SWCNTs and $(OH)_4$PcHH in water, dimethylformamide (DMF), and dimethylsulfoxide (DMSO), respectively. Threshold values did not exceed 100 mJ/cm^2. The Z-scan showed a gradual decrease in the duration of the laser pulse by 53%; however, near the focus, there was a sharp increase in the duration of the transmitted pulse, reaching a value of 29 ns in z = 0. This phenomenon confirms the occurrence of reverse saturable absorption in the investigated media and can be used in photonic devices to control the temporal characteristics of the signal. Thus, the possibility of protection of sensitive photonic devices and human eyes from nanosecond laser pulses in the near UV range by nanodispersed liquid media based on composites of SWCNTs with $(OH)_4$PcHH has been discussed in this paper.

Keywords: laser protection; nonlinear optics; UV radiation; Z-scan; carbon nanotubes; phthalocyanines

Citation: Vasilevsky, P.N.; Savelyev, M.S.; Tolbin, A.Y.; Kuksin, A.V.; Vasilevskaya, Y.O.; Orlov, A.P.; Shaman, Y.P.; Dudin, A.A.; Pavlov, A.A.; Gerasimenko, A.Y. Nonlinear Optical Response of Dispersed Medium Based on Conjugates Single-Walled Carbon Nanotubes with Phthalocyanines. *Photonics* **2023**, *10*, 537. https://doi.org/10.3390/photonics10050537

Received: 19 April 2023
Revised: 28 April 2023
Accepted: 3 May 2023
Published: 6 May 2023

1. Introduction

Since the invention of the laser in the 1960s, laser radiation is increasingly being used in various fields [1]. Devices for laser welding [2], photolithography systems [3], industrial lasers, laser surgical complexes, vision correction devices [4], laser designators,

and rangefinders [5] are actively used in everyday practice. In recent years, the direction of laser communication systems and laser scanning using LiDARs has been developing [6]. Most laser systems operate in the near UV to near IR range. This is due to the wide availability of lasers and the ability to detect the signal with low-cost Si detectors.

The development of laser technologies and the growth of laser radiation power has highlighted the problem of effective protection for photosensitive detectors and human vision [7]. For a human, radiation of the invisible range is especially dangerous, since the retina of the eye is not sensitive to such radiation. As a result, information about the signal does not enter the brain, which leads to a significant slowdown in the reflex reaction (or its complete absence) to high-intensity laser radiation. In addition, UV radiation is well absorbed by organic compounds, and the impact of laser pulses can lead to retinal burns or damage to the crystalline lens [8,9].

To provide effective protection against high-intensity laser radiation, optical limiters based on nonlinear optical effects can be used [10,11]. Such devices provide a high level of visual control (linear transmittance > 60%) when the radiation intensity is below the threshold value, but when the threshold is exceeded, the nonlinear absorbers "darken out", which leads to a limitation of the output signal.

There are various materials that can be used as a non-linear optical limiter, such as metal nanoparticles [12], organic dyes [13], carbon nanomaterials (carbon dots [14], fullerenes, carbon nanotubes [15], etc.), complex nanoparticles [16] and others. The advantage of using carbon materials is the possibility of obtaining a nonlinear attenuation of laser radiation in a wide range of wavelengths [17], particularly in the ultraviolet range [18,19]. However, their use is limited due to relatively poor dispersibility [19,20]. For this reason, it is necessary to create composites with carbon nanomaterials, which are easier to disperse in water or other common organic solvents [19,21]. Additionally, the conjugation of carbon nanomaterials with different functionalization strategies [20,22] increases the nonlinear response. In this case, it is necessary to control the size of agglomerates [18], and, in the case of carbon nanotubes, the size of their bundles [21]. Among the materials that provide perfect nonlinear absorption, phthalocyanines occupy an important place. The phthalocyanine molecule is an 18 π-conjugated macroheterocyclic dye, the chemical modification of which makes it easy to tune the nonlinear optical properties for a specific task [23–26]. The phthalocyanine has an ultrafast response time, which effectively limits pico- and nanosecond pulses [27,28]. Due to the manifestation of a nonlinear optical absorption itself, phthalocyanines can be conjugated with various types of nanoparticles to enhance the nonlinear response [29–32]. To preserve the advantages of modifying their structure, it is necessary to take into account their tendency to aggregation, which, in the case of a ligand, has a minimal effect on the nonlinear optical properties [33]. Phthalocyanines have a low limiting threshold. The conjugation of the carbon nanomaterials with phthalocyanines made it possible to reduce the limiting threshold and, consequently, increase the speed of switching on the limiting [34]. Single-walled carbon nanotubes (SWCNTs) are strips of graphite monolayers (graphene) rolled into cylinders [35]. SWCNTs are promising materials for optical limiting since they have strong nonlinear properties and high photo- and thermal stability [36–39]. The SWCNTs have a specific absorption spectrum depending on their structural topology and chirality. However, the use of unsorted SWCNTs makes it possible to achieve a high level of visual control over a wide wavelength range without pronounced absorption peaks [40]. The nonlinear optical (NLO) properties of carbon nanoparticles and their conjugates with organic dyes are known in the visible and near IR ranges [34]; however, the response is still poorly understood in the UV range.

This paper presents a study of the nonlinear optical properties of liquid disperse media of SWCNT/metal-free tetra(hydroxy)phthalocyanine $(OH)_4$PcHH) composite ($(OH)_4$PcHH @ SWCNT). The paper describes the synthesis of the dye, nanocomposites, the process of preparing dispersions, and NLO research. Water, dimethylformamide (DMF), and dimethyl sulfoxide (DMSO) were used as solvents. The nanoparticle concentration is chosen so that the linear transmission was above 60% at 355 nm. The third harmonic of

a nanosecond Nd:YAG laser LS-2147N(5) (Lotis TII, Belarus) (355 nm, 20 ns) was used to study NLO parameters using Z-scan and fixed sample position experiments. Additionally, Z-scan was used to determine the change in the width of a laser pulse passing through a sample. The studied materials showed a threshold value in the range of 0.04–0.06 J/cm^2 and strong optical limiting characteristics that make such materials promising for limiting UV laser radiation.

2. Materials and Methods

2.1. Synthesis and Characterization

To synthesize starting metal-free phthalocyanine, 160 mg of lithium methoxide (Scheme 1) was added to a solution of 4-benzyloxyphthalonitrile **1** (200 mg, 0.85 mmol) in n-hexanol (30 mL). The mixture was first stirred at room temperature (10 min), and then refluxed for 6 h. After completion, the reaction mixture was evaporated under reduced pressure, conc. H_2SO_4 was added to the semi-solid residue and poured onto ice. The phthalocyanine precipitate was filtered off and washed several times with methanol. The chromatography was carried out on SiO_2 (Merck, 40 × 63 mkm), eluent—THF. A total of 74 mg of ligand **2** was obtained (yield 60%). MALDI-TOF (HCCA matrix): *m*/*z* 578.30 $[M]^+$, calcd. for $[C_{32}H_{18}N_8O_4]$ 578.55; UV-vis (THF), λ_{max}/nm (log ε): 289 (3.57), 340 (3.71), 389 (3.42), 670 (3.84), 706 (3.83); UV-vis (DMF), λ_{max}/nm (log ε): 297 (3.66), 345 (3.76), 425 (3.41), 670 (3.89), 704 (3.95). The spectra are presented in Figure 1.

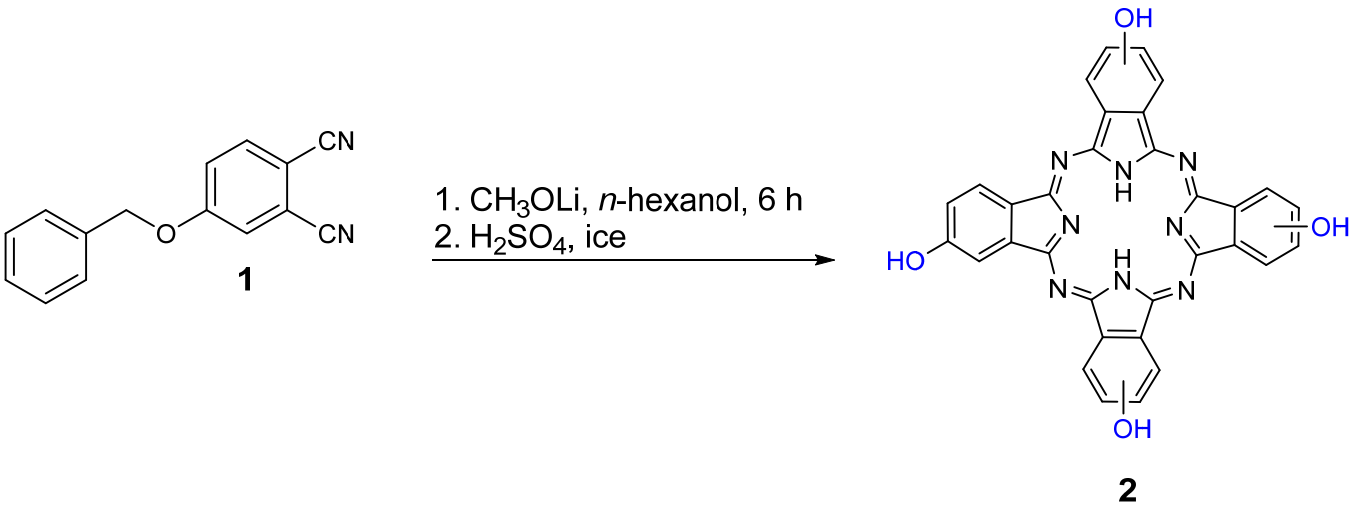

Scheme 1. Scheme for the synthesis of free-metal phthalocyanines $(OH)_4$PcHH.

For binding phthalocyanine **2** to carbon nanotubes, SWCNTs were preliminarily functionalized with carboxyl groups. A suspension of SWCNTs was boiled in concentrated HNO_3 for 6 h, and then the material was filtered and washed with water until neutral.

Next, phthalocyanine **2** (25 mg) was added to a suspension of SWCNT-COOH (50 mg) in DMF (50 mL), and the mixture was subjected to ultrasonic treatment for 30 min (Scheme 2). After that, bis-1,2-(bromomethyl)benzene (10 mg) and 1,8-Diazabicyclo(5.4.0)undec-7-ene (DBU) (0.1 mL) were added. The mixture was boiled for 30 min, after which the solid mass was centrifuged and washed many times in tetrahydrofuran (THF) to remove unreacted **2** and oligomeric phthalocyanine products. The weight of the material increased by 21 mg after synthesis, from which it can be concluded that the reaction was complete and by-products were formed in insignificant amounts. According to dynamic light scattering (DLS) data, the hydrodynamic radius increased from 288 ± 55 nm to 350 ± 60 nm after the reaction.

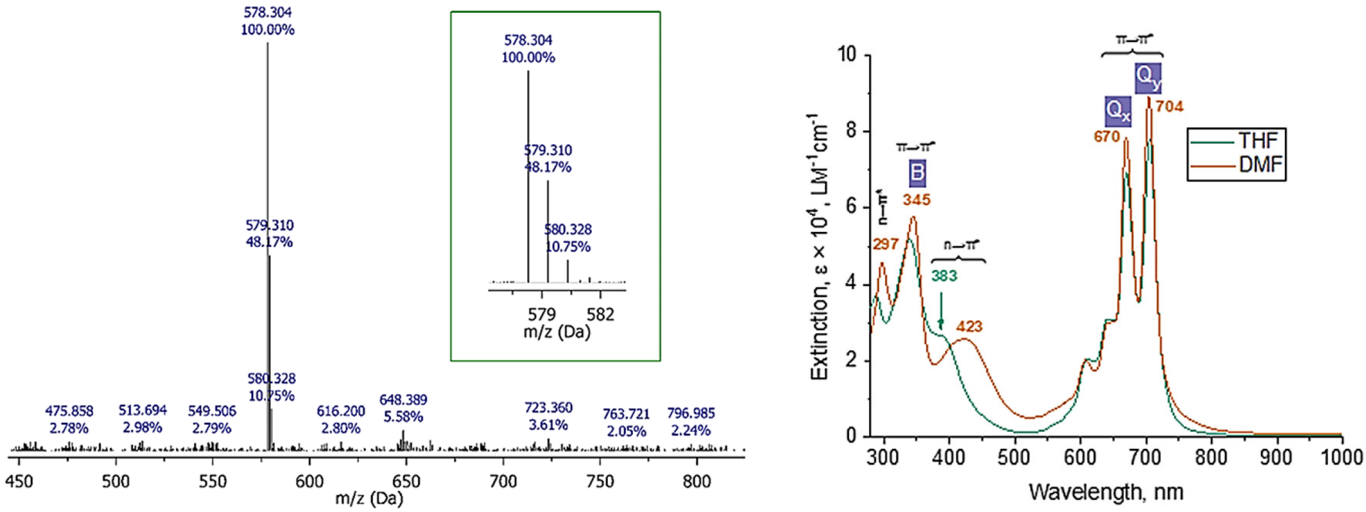

Figure 1. MALDI-TOF (matrix—HCCA) mass spectrum (**a**) and UV-vis spectra of dye **2** (**b**).

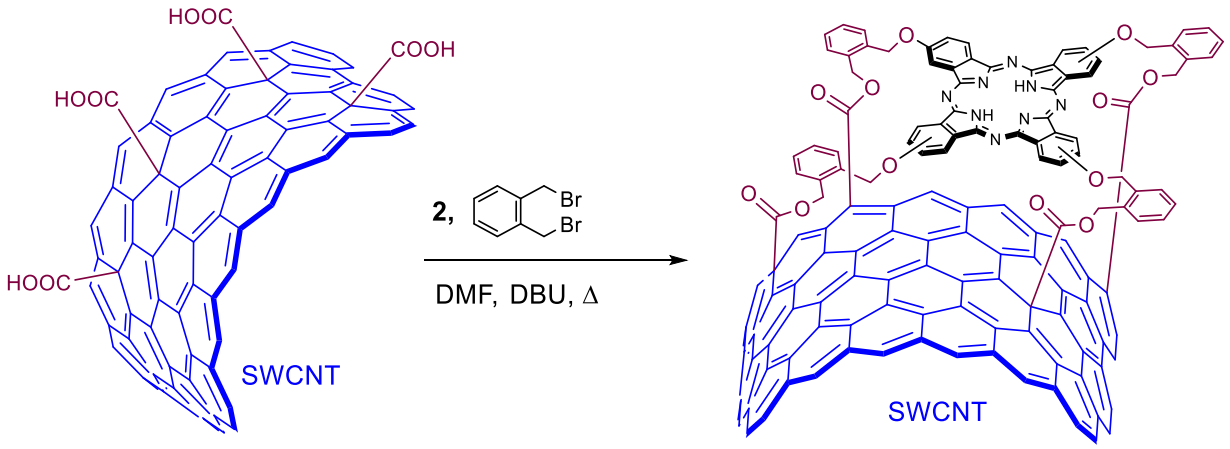

Scheme 2. Synthesis of composite $(OH)_4$PcHH @ SWCNT.

To prepare liquid media, 0.01 wt% of $(OH)_4$PcHH @ SWCNT powder was added to 50 mL of the following solvents: water, DMF, and DMSO. Then, the resulting suspensions were processed in a Soniqator Q700 ultrasonic homogenizer (Qsonica, Newtown, CT, USA) at 30 W and 40% amplitude for 1 h to achieve dispersion uniformity. The temperature of the dispersions during ultrasonic homogenization was controlled and did not exceed 40 °C. Centrifugation at 1000 rpm was performed for 10 min to remove large unmixed agglomerates.

To characterize the quality of the synthesized nanoparticles, thin films were obtained by the spray deposition method. The airflow supply pressure was 20 bar. The pressure for supplying the dispersion was 0.05 bar. The nozzle diameter was 0.5 mm. Silicon substrates were clamped in a holder and placed on a heating table (100 °C) for accelerated evaporation of the solvent from the formed layer.

2.2. Characterisation of Composites

The structure of the obtained $(OH)_4$PcHH @ SWCNT composites was studied using the SEM method. The DLS method (Photocor, Moscow, Russia) was used to determine the hydrodynamic radius of composites in various solvents. A GENESYS 50 UV-Vis spectrophotometer (Thermo Fisher Scientific, Waltham, MA, USA) was used to evaluate the linear transmission in the range from 300 to 1100 nm.

Next, the carboxylation of SWCNTs was confirmed by the Raman spectrum (Figure 2). A Confocal Raman microscope InVia Qontor (Renishaw, Wotton-under-Edge, UK) was used to record Raman scattering spectra. As an excitation radiation source, the laser with a wavelength of 532 nm was utilized. During the measurements, a 50× objective for the visible range and a diffraction grating of 1200 lines/mm were used.

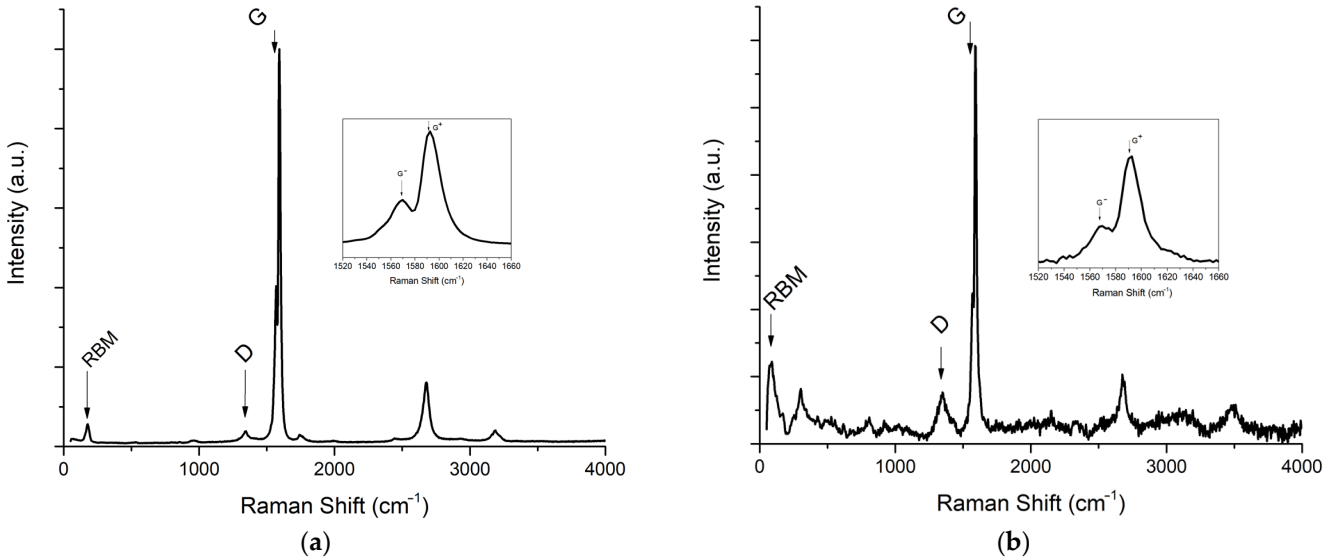

Figure 2. Raman spectrum for SWCNTs (**a**) and SWCNT-COOH (**b**).

For initial SWCNTs, the RBM mode is presented as a broad band with a maximum of 185 cm^{-1} and a shoulder around 152, 162, and 176 cm^{-1}. This indicates the presence of SWCNTs with different chirality, which results in the superposition of modes from each type of SWCNT and the appearance of one broad mode [41]. The semiconductor nanotubes prevail, as evidenced by the splitting of the G mode into a high-intensity peak G^+ (1591 cm^{-1}) and a low-intensity G^- (1570 cm^{-1}). The I_D/I_G ratio was 0.038, which indicates a small defectiveness of the initial SWCNTs. The Raman spectrum of SWCNT-COOH has RBM modes around 139, 179, 239, and 293 cm^{-1}, which indicates the presence of the tubes with different chirality and different diameters. At the same time, the frequencies of RBM differ in comparison with the initial SWCNTs, which is probably due to the effect of the functionalization of COOH groups during acid treatment. In this case, nanotubes are damaged upon the attachment of side functional groups [42]. Functionalization does not change the type of conductivity (semiconductor type), which is confirmed by the splitting of the G mode, similar to the spectrum of the original SWCNTs: G^+ (1593 cm^{-1}) and G^- (1570 cm^{-1}). A small shift of G^+ and D (1350 cm^{-1}) in frequency in comparison with the initial SWCNTs can also be explained by the functionalization of COOH groups.

2.3. NLO Studies

The third harmonic of a nanosecond Nd:YAG pulsed laser (355 nm) was used to study the nonlinear optical response of the obtained dispersed media. The width of the generated pulse was ~20 ns; the spatial profile of the beam had a Gaussian shape.

To measure the third-order nonlinear optical absorption coefficient, threshold intensity, and attenuation coefficient, experiments were carried out using the Z-scan method and the method of the fixed position of the material [43]. These methods are based on changing the input fluence by varying the laser beam radius or laser radiation energy correspondingly. For Z-scan, the step between measurements was 0.5 mm. Irradiation was performed in a single pulse mode at each position of the sample. The time between laser pulses was 2 s. The pulse energy during Z-scan was 100 μJ. The thickness of the samples was 3 mm. A Glan-Taylor polarization prism and a closed variable wheel attenuator (Standa, Vilnius, Lithuania) were used to change the energy of the incident pulse. PE9-C detectors (Ophir,

Jerusalem, Israel) were used to register the energy of input and output pulses. Laser radiation was focused on the sample using a lens with a focal length of 15 cm. The beam radius before focusing was ~0.8 mm. Si PIN-photodiodes OD-08A (Avesta Project, Moscow, Russia) and an MSO64 oscilloscope (Tektronix, Beaverton, OR, USA) were used to record the duration of input and output nanosecond pulses.

3. Results and Discussion

3.1. Spectral Properties of Dye 2

Figure 1b shows the UV-vis spectra of phthalocyanine **2**, which demonstrate a high spectral response ($\varepsilon > 80{,}000$ $LM^{-1}cm^{-1}$) in THF and DMF solvents. Absorption bands in the near-boundary with the near-IR range (600–700 nm) are related to π–π* electronic transitions. A small low-intensity shoulder at 383 nm in THF indicates the presence of hydroxy groups, which are n–π* transitions. The absorption region of 350–500 nm is more pronounced in DMF, which is associated with the basicity of the solvent and the possible ionization of peripheral hydroxyl groups. That is why DMF was chosen as the solvent for carrying out the crosslinking reaction (Scheme 2), and DBU was added to the suspensions to increase the basicity of the medium.

3.2. SEM Study

Analysis of SEM images of initial SWCNTs showed the presence of individual nanofibers with a diameter of ~15 nm (Figure 3a,b). The length of nanofibers varies and can reach 5 μm. Enlarged images show that SWCNTs tend to curl, which can lead to the appearance of large agglomerates in liquid dispersions [44].

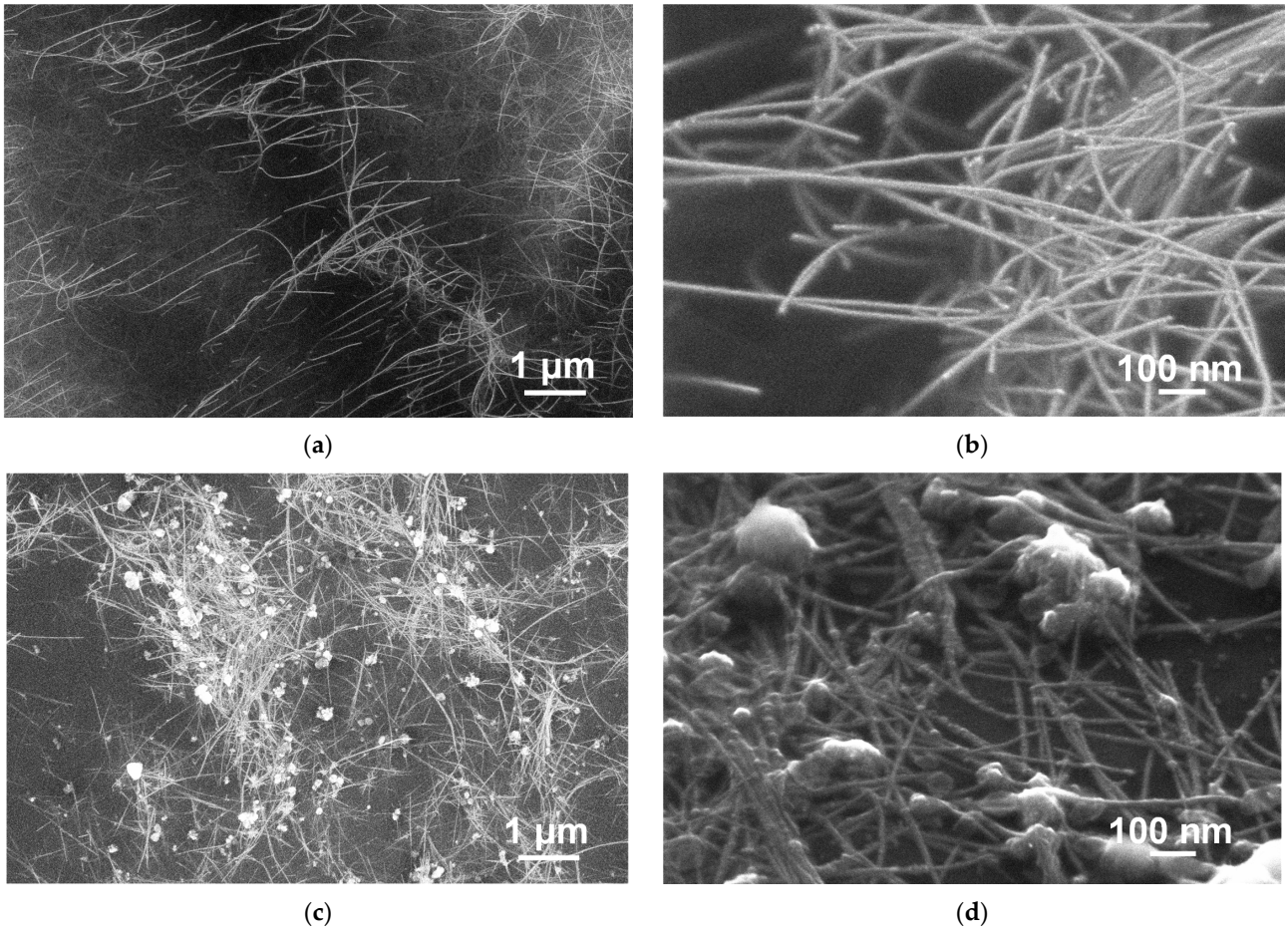

Figure 3. SEM images of the initial SWCNTs (**a**,**b**) and $(OH)_4$PcHH @ SWCNT composites (**c**,**d**) in different scales.

The binding of phthalocyanine **2** to SWCNTs is demonstrated by the inclusion of spherical nanoclusters in their structure (Figure 3c,d). Their sizes average ~40–50 nm but can reach higher values (~200 nm). SEM images show that large clusters of phthalocyanine are able to settle on several SWCNTs fibers as if cross-linking them. The binding strength of phthalocyanine **2** is quite high, which is confirmed by the impossibility of eliminating nanoclusters even with boiling DMF. Based on this, we can assume that the dye is covalently bound to SWCNTs and exclude its simple adsorption.

3.3. Dynamic Light Scattering

The DLS study was performed 24 h after the generation of the $(OH)_4$PcHH @ SWCNT dispersions. This was performed in order to evaluate the degree of aggregation of composite particles in different solvents. The results of the DLS study are shown in Table 1.

Table 1. DLS study on $(OH)_4$PcHH @ SWCNT composites in solvents.

Solvent	Type of Particles	Hydrodynamic Radius, nm	Standard Deviation, nm	Contribution, %
Water	Separated nanoparticles	347	55	31
	Agglomerates	21,000	8700	69
DMF	Separated nanoparticles	342	52	92
	Agglomerates	15,000	3800	8
DMSO	Separated nanoparticles	352	60	93
	Agglomerates	17,000	5600	7

DLS results show that large agglomerates of nanoparticles (with a hydrodynamic radius of more than 20 μm) were formed in large quantities in the water dispersion. The contribution to the total scattering of such particles was 69%. The contribution of such particles to the scattering was only 8 and 7% for DMF and DMSO dispersions, respectively. This allows us to conclude that the $(OH)_4$PcHH @ SWCNT composites in water dispersion tend to aggregate faster, which leads to a deterioration in the stability of the dispersion. The hydrodynamic radius of separated nanoparticles was ~350 ± 60 nm for all three solvents.

3.4. NLO Measurements

The linear optical transmission spectra of dispersions with pure SWCNTs and $(OH)_4$PcHH @ SWCNT composites were recorded in a quartz cell with an optical path length of 3 mm (Figure 4). A small signal in the range of 680–690 nm is associated with the absorption of phthalocyanine. It can be noted that the dispersion spectra are quite uniform and have a high transmission (more than 60%) in the range of 350–1100 nm. This indicates the presence of SWCNTs with unspecified topology and chirality in the resulting dispersions [45]. The linear transmission at a wavelength of 355 nm was ~64–66% for all dispersions, which indicates the similarity of their linear optical properties.

To study the nonlinear optical response, open-aperture Z-scan and the experiment with fixed sample position were performed. The studies were carried out in the range from −35 to 35 mm relative to the focus of the lens. Figure 5 shows the Z-scan curves of pure SWCNTs, $(OH)_4$PcHH, and $(OH)_4$PcHH @ SWCNT composites in water, DMF, and DMSO. Since phthalocyanines are insoluble in water, results are shown for DMF and DMSO solutions. The solid lines on the charts show theoretical fits, which were obtained by the processing of the experimental data with the "threshold" model [46]. The threshold model provides the plotting of theoretical curves for various optical coefficients and comparison with experimental data. Such processing based on radiation transfer equation allows calculating nonlinear optical parameters such as third-order nonlinear absorption coefficient and limiting threshold. The last parameter is especially important in the study of materials with a pronounced nonlinear threshold effect. The Z-scan results for $(OH)_4$PcHH solutions were analyzed with a nonlinear absorption model that considers saturable absorption [47].

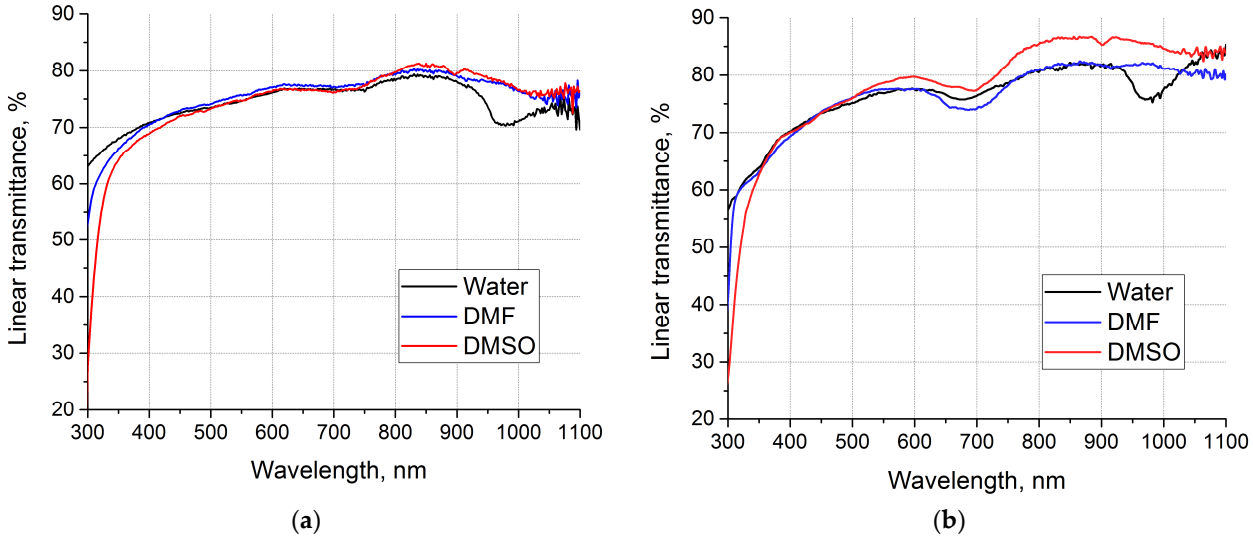

Figure 4. Linear transmittance spectra of pure SWCNTs (**a**) and $(OH)_4$PcHH @ SWCNT composites (**b**) in different solvents.

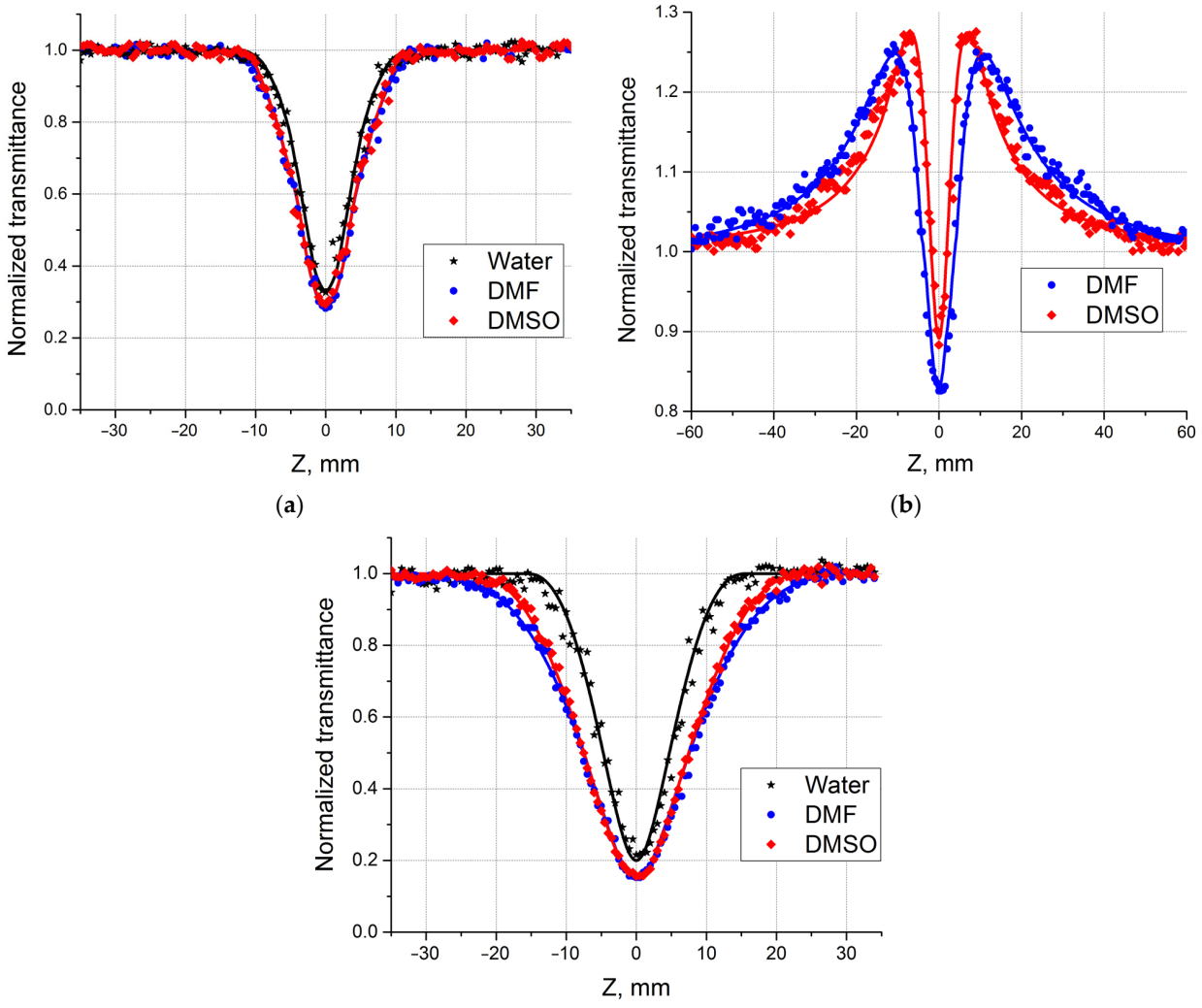

Figure 5. Z-scan curves of pure SWCNTs (**a**), $(OH)_4$PcHH (**b**), and $(OH)_4$PcHH @ SWCNT composite (**c**) in different solvents.

The Z-scan curves for SWCNTs dispersions clearly demonstrate that the normalized transmission starts to decrease when a certain position of the sample on the Z-axis is reached and reaches its minimum value at the focus of the lens (z = 0). After passing through the focus, the normalized transmission increased again and reached the value of 1 for all the studied samples. The Z-scan curves are symmetrical with respect to the lens focus, which indicates the absence of the contribution of extraneous nonlinearities associated, among other things, with the used optical equipment. The curves for the dispersions of pure SWCNTs in DMF and DMSO nearly overlap with each other, which indicates the similarity of the nonlinear optical properties of the dispersions. The water dispersion showed a lower attenuation coefficient in the focus compared to the dispersions of DMF and DMSO.

The curves for $(OH)_4$PcHH solutions showed a different behavior (Figure 5b). The samples showed enlightenment far from the focus. This indicates the manifestation of saturable absorption. The sharp drop in the normalized transmission is observed at the focus of the lens; however, it is much smaller compared to SWCNTs dispersions.

The water dispersion of $(OH)_4$PcHH @ SWCNT composite showed the least limitation in the focus of the lens at the same parameters of the incident laser radiation. It is also worth noting that fluctuations in experimental values are typical for water dispersion. This may be due to the effects of scattering on large agglomerates [48,49]. The uneven distribution of nanoparticles due to aggregation leads to a decrease in the nonlinear optical response of the water dispersion. The DMF and DMSO dispersions showed approximately the same attenuation at the focus of the lens. The transition to nonlinear attenuation starts a little earlier for the DMF dispersion, which indicates a lower value of the limiting threshold [50]. There are practically no fluctuations in the experimental data for DMF and DMSO dispersions.

Figure 6 shows the output pulse width as a function of Z displacement. The input pulse width was determined by the 1/2 level and was 20 ns.

While the sample moved closer to the focus, the output pulse width started to change. This change occurred simultaneously with a decrease in the normalized transmission. For pure SWCNTs dispersions, the output pulse width gradually decreased and reached a minimum (10~12 ns) at Z = 0 mm. The change in the pulse width for the $(OH)_4$PcHH solutions started only with a decrease in the normalized transmission, and enlightenment had no influence.

A different trend was observed for dispersions of $(OH)_4$PcHH @ SWCNT composite. The output pulse width was reduced to ~10 ns for the studied samples. Then, immediately near the focus, the pulse width sharply increased and reached values of 22.5, 28, and 29 ns for water, DMF, and DMSO dispersions, respectively. The comparison of Figures 5 and 6 shows that the transition to an increase in the pulse duration occurs when the normalized transmission reaches the value of ~0.3.

Additionally, input-output curves were obtained during the fixed sample position experiment for $(OH)_4$PcHH @ SWCNT composites in different solvents. For this purpose, the samples were placed at the focus of the lens, with the input laser pulse fluence being varied in the range of 0–2.5 J/cm^2. The beam radius at the lens focus was ~75 μm. The results are presented in Figure 7. Similarly to the Z-scan, the water dispersion of $(OH)_4$PcHH @ SWCNT composites exhibited the worst nonlinear optical limiting. The DMF and DMSO dispersions showed almost identical limiting properties, which are in good agreement with the Z-scan data.

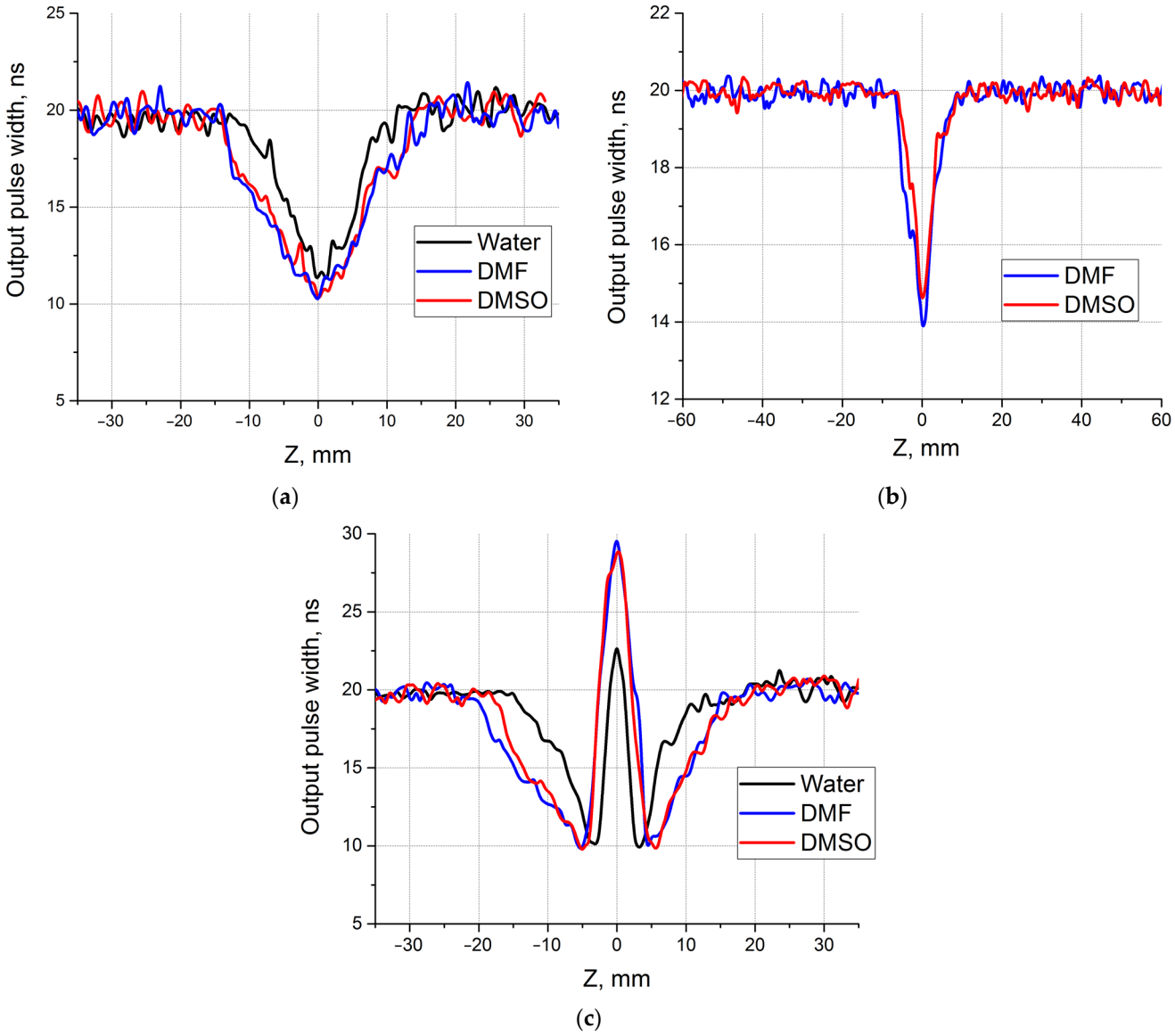

Figure 6. Output pulse width dependence on Z displacement for pure SWCNTs (**a**), $(OH)_4$PcHH (**b**), and $(OH)_4$PcHH @ SWCNT composite (**c**) in different solvents.

Based on the results of the NLO study, the following optical parameters of $(OH)_4$PcHH @ SWCNT composites were calculated: linear and third-order nonlinear optical absorption coefficients, limiting threshold, and attenuation coefficient (Table 2). $(OH)_4$PcHH solutions showed the lowest attenuation coefficient and enlightenment far from focus, which indicates low limiting properties. However, phthalocyanines can be used to enhance the nonlinear optical limiting of SWCNTs. $(OH)_4$PcHH @ SWCNT composites have higher values of the third-order nonlinear optical absorption coefficient in comparison with the dispersions of the initial SWCNT. The low limiting threshold for DMF and DMSO dispersions is explained by a more uniform distribution of nanoparticles in the material, while large agglomerates in water dispersion become saturated more slowly. This is due to the fact that they are also capable of scattering laser radiation, in addition to absorbing photons. This can be confirmed by fluctuations in the experimental values during the Z-scan and fixed sample position experiment for water dispersions. The linear absorbance calculated with the NLO study is in good agreement with the spectrophotometric data.

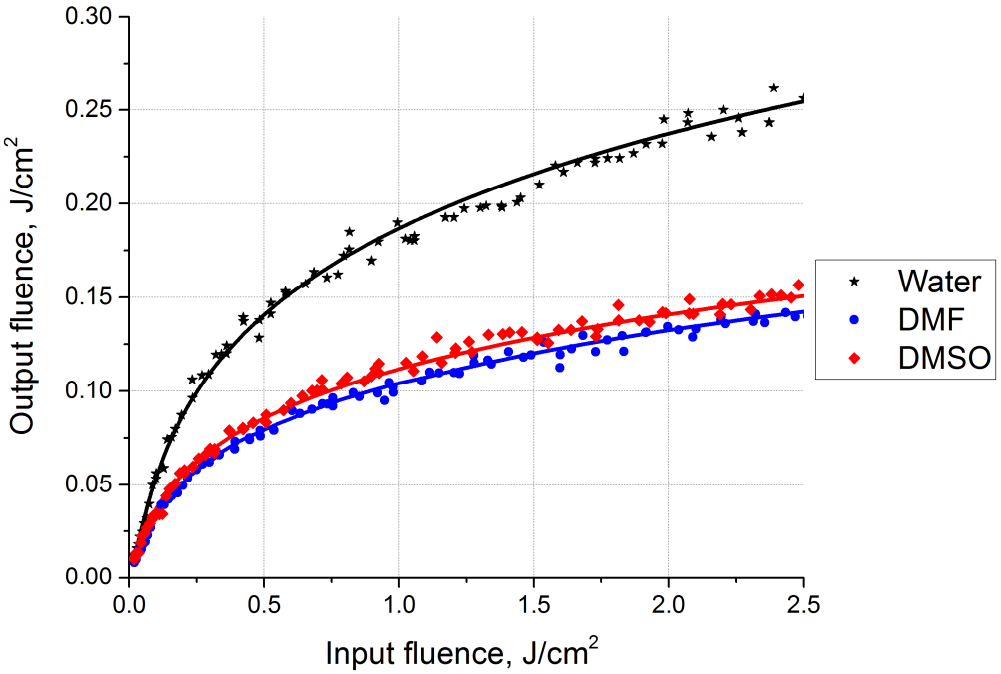

Figure 7. Input-output dependence curves of $(OH)_4$PcHH @ SWCNT composites in different solvents.

Table 2. Calculated optical parameters for nanoparticles in different solvents.

Nanoparticles	Solvent	Linear Transmittance, %	Linear Absorption Coefficient, cm^{-1}	Third-Order Nonlinear Optical Absorption Coefficient, cm/GW	Limiting Threshold, J/cm^2	Attenuation Coefficient
Initial SWCNT	Water	64.5 ± 0.5	1.47 ± 0.02	76 ± 4	0.20 ± 0.03	3.15 ± 0.15
	DMF	63.9 ± 0.5	1.50 ± 0.02	108 ± 4	0.17 ± 0.02	3.80 ± 0.15
	DMSO	64.1 ± 0.5	1.49 ± 0.02	105 ± 4	0.17± 0.02	3.79 ± 0.15
$(OH)_4$PcHH	Water			Not soluble		
	DMF	44.8 ± 0.5	2.69 ± 0.03	10 ± 1	0.75 ± 0.03	1.11 ± 0.02
	DMSO	45.1 ± 0.5	2.67 ± 0.03	6 ± 1	0.85 ± 0.03	1.20 ± 0.04
Composites $(OH)_4$PcHH @ SWCNT	Water	64.5 ± 0.5	1.47 ± 0.02	149 ± 5	0.09 ± 0.02	4.95 ± 0.15
	DMF	63.6 ± 0.5	1.52 ± 0.03	236 ± 6	0.05 ± 0.02	6.52 ± 0.15
	DMSO	63.8 ± 0.5	1.51 ± 0.02	229 ± 6	0.06 ± 0.02	6.51 ± 0.15

4. Discussion

The resulting composites $(OH)_4$PcHH @ SWCNT composites can be used as nonlinear media in passive optical limiters. The binding of phthalocyanine molecule to the single-walled carbon nanotube enhances its nonlinear absorption, which can be explained by the combined nonlinear optical response from SWCNTs and the phthalocyanine dye $(OH)_4$PcHH [51]. When photons are absorbed, photoinduced energy transfer from phthalocyanine to SWCNT may occur [30,52]. The transfer of excited electrons from phthalocyanine to SWCNT leads to its faster manifestation of reverse saturable absorption, which leads to optical limiting. It also explains a decrease in the values of the limiting threshold for the dispersions of $(OH)_4$PcHH @ SWCNT composites compared to pure SWCNTs dispersion.

The effect of changing the pulse width can also be explained in terms of the reverse saturable absorption [53]. The output pulse width curve can be divided into three regions (Figure 8a). In area I, the output pulse has a Gaussian temporal profile (Figure 8b). This area is characterized by a linear interaction of the laser pulse with the medium. The pulse fluence is not enough to induce nonlinear absorption. When approaching the focus, a transition to a nonlinear interaction occurs. The leading edge of the beam saturates the medium, interacting with it linearly. The trailing edge of the beam already passes through a saturated medium and thus experiences nonlinear absorption (area II). Near the focus

(±4 mm from the focus), the intensity becomes high enough for the leading edge of the pulse to experience nonlinear absorption (area III). This leads to a sharp drop in the peak intensity of the pulse.

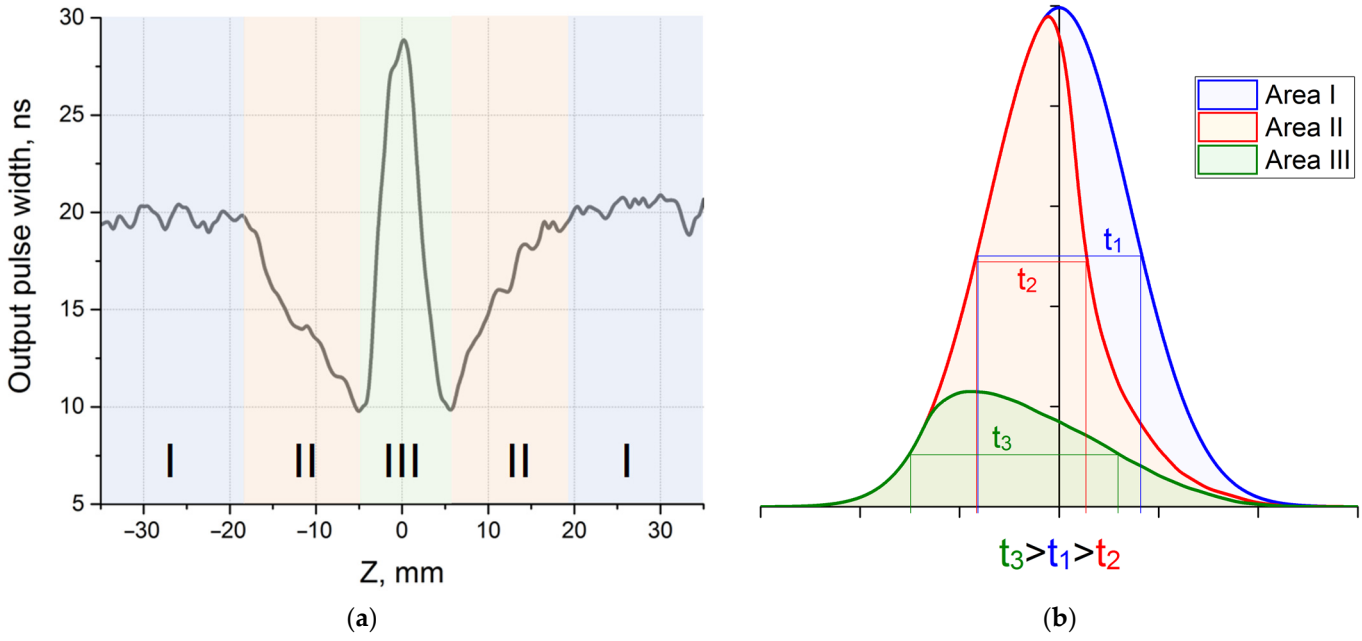

(**a**) (**b**)

Figure 8. Output pulse width dependence on Z displacement for $(OH)_4$PcHH @ SWCNT composites in DMSO (**a**) and temporal beam profile for corresponding areas (**b**).

Thus, when the pulse width is determined from the 1/2 level, a sharp increase in the width of the output pulse is observed. Such a change in the width of the output laser pulse shows that the main limiting effect in liquid dispersions of $(OH)_4$PcHH @ SWCNT composites is reverse saturable absorption. In the case of the dispersion of pure SWCNTs, the nonlinear optical response is much smaller, so there is no increase in the output pulse width. Based on the comparison of Z-scan curves and output pulse width dependence, it can be assumed that the increase in the output pulse width occurs when the normalized transmission decreases below the value of 0.3.

5. Conclusions

Composites $(OH)_4$PcHH @ SWCNT were synthesized and their dispersions in water, DMF, and DMSO were investigated. SEM images confirmed the inclusion of phthalocyanine **2** molecules in the carbon nanomaterial. Nonlinear optical parameters of composites were calculated from the Z-scan and input-output curves. The water dispersion is characterized by the presence of large agglomerates, and this leads to deterioration in stability and nonlinear optical response. The introduction of $(OH)_4$PcHH dye into SWCNTs leads to an increase in the third-order nonlinear optical absorption coefficient and a decrease in the limiting threshold, while $(OH)_4$PcHH solutions show low optical limiting itself at 355 nm. The change in the width of the output pulse is also shown, which allows us to conclude that the main effect leading to the limitation of the laser pulse fluence in the studied materials is reverse saturable absorption. The obtained results suggest that media based on $(OH)_4$PcHH @ SWCNT composites can be a good choice for creating eye and photosensitive sensors protection from nanosecond UV laser radiation.

Author Contributions: Conceptualization, A.Y.G. (Alexander Yu. Gerasimenko); methodology, A.Y.T. (Alexander Yu. Tolbin) and A.Y.G. (Alexander Yu. Gerasimenko); validation, A.P.O. and A.Y.G. (Alexander Yu. Gerasimenko); formal analysis, M.S.S.; investigation, P.N.V., A.V.K., Y.O.V. and A.P.O.; resources, A.Y.T. (Alexander Yu. Tolbin), A.A.P. and A.A.D.; data curation, P.N.V. and M.S.S.; writing—original draft preparation, P.N.V., A.V.K. and Y.O.V.; writing—review and editing, M.S.S., A.Y.T. (Alexander Yu. Tolbin), Y.P.S. and A.Y.G. (Alexander Yu. Gerasimenko); visualization, P.N.V. and A.Y.G. (Alexander Yu. Gerasimenko); supervision, A.Y.G. (Alexander Yu. Gerasimenko); project administration, A.Y.G. (Alexander Yu. Gerasimenko), A.A.P. and A.A.D.; funding acquisition, A.Y.T. (Alexander Yu. Tolbin), A.A.P. and A.Y.G. (Alexander Yu. Gerasimenko). All authors have read and agreed to the published version of the manuscript.

Funding: Syntheses of phthalocyanine dye **2** and corresponding composite with SWCNT were carried out with the financial support of the Russian Science Foundation (Grant 21-73-20016). The MALDI-TOF and UV-vis measurements were performed within the framework of the State Assignment of 2022 («Creation of compounds with given physicochemical properties», No. FFSN-2021-0003). The main research concerning the protection of electro-optical systems and organs of vision due to optical limiting was supported by the Ministry of Industry and Trade of the Russian Federation (State contract No. 20411.1950192501.11.003 from 29 December 2020, identifier 17705596339200009540).

Institutional Review Board Statement: Not applicable.

Informed Consent Statement: Not applicable.

Data Availability Statement: Data underlying the results presented in this paper are not publicly available at this time but may be obtained from the corresponding authors upon reasonable request.

Conflicts of Interest: The authors declare no conflict of interest.

References

1. Bertolotti, M. *The History of the Laser*; CRC Press: Boca Raton, FL, USA, 2004; p. 316. [CrossRef]
2. Acherjee, B. Hybrid laser arc welding: State-of-art review. *Opt. Laser Technol.* **2018**, *99*, 60–71. [CrossRef]
3. Zhang, Q.; Lee, Y.H.; Phang, I.Y.; Lee, C.K.; Ling, X.Y. Hierarchical 3D SERS Substrates Fabricated by Integrating Photolithographic Microstructures and Self-Assembly of Silver Nanoparticles. *Small* **2014**, *10*, 2703–2711. [CrossRef]
4. Khalkhal, E.; Rezaei-Tavirani, M.; Zali, M.R.; Akbari, Z. The evaluation of laser application in surgery: A review article. *J. Lasers Med. Sci.* **2019**, *10*, S104. [CrossRef]
5. Amann, M.C.; Bosch, T.M.; Lescure, M.; Myllylae, R.A.; Rioux, M. Laser ranging: A critical review of unusual techniques for distance measurement. *Opt. Eng.* **2001**, *40*, 10–19. [CrossRef]
6. Raj, T.; Hanim Hashim, F.; Baseri Huddin, A.; Ibrahim, M.F.; Hussain, A. A survey on LiDAR scanning mechanisms. *Electronics* **2020**, *9*, 741. [CrossRef]
7. Geis, M.W.; Bos, P.J.; Liberman, V.; Rothschild, M. Broadband optical switch based on liquid crystal dynamic scattering. *Opt. Express* **2016**, *24*, 13812–13823. [CrossRef]
8. Barkana, Y.; Belkin, M. Laser eye injuries. *Surv. Ophthalmol.* **2000**, *44*, 459–478. [CrossRef]
9. Ivanov, I.V.; Mappes, T.; Schaupp, P.; Lappe, C.; Wahl, S. Ultraviolet radiation oxidative stress affects eye health. *J. Biophotonics* **2018**, *11*, 201700377. [CrossRef]
10. Dini, D.; Calvete, M.J.F.; Hanack, M. Nonlinear optical materials for the smart filtering of optical radiation. *Chem. Rev.* **2016**, *116*, 13043–13233. [CrossRef]
11. Kaniyarakkal, S.; Thomas, T.; Sadagopalan, S.K.; Jayamohan, L.; Muralimanohar, R.; Vasanthakumaryamma, L.; Sadasivan Nair, V. Synthesis, Linear and Nonlinear Optical Properties of Ag/Al_2O_3 Nanocomposites. *Materials* **2022**, *15*, 6322. [CrossRef]
12. Zhang, Y.; Wang, Y. Nonlinear optical properties of metal nanoparticles: A review. *RSC Adv.* **2017**, *7*, 45129–45144. [CrossRef]
13. Yahya, M.; Nural, Y.; Seferoğlu, Z. Recent advances in the nonlinear optical (NLO) properties of phthalocyanines: A review. *Dyes Pigment.* **2022**, *198*, 109960. [CrossRef]
14. Nancy, P.; Joy, N.; Valluvadasan, S.; Philip, R.; Thomas, S.; Antoine, R.; Kalarikkal, N. Fluorescence and Nonlinear Optical Response of Graphene Quantum Dots Produced by Pulsed Laser Irradiation in Toluene. *Molecules* **2022**, *27*, 7988. [CrossRef]
15. Gadhwal, R.; Devi, A. A review on the development of optical limiters from homogeneous to reflective 1-D photonic crystal structures. *Opt. Laser Technol.* **2021**, *141*, 107144. [CrossRef]
16. Nancy, P.; Jose, J.; Joy, N.; Valluvadasan, S.; Philip, R.; Antoine, R.; Thomas, S.; Kalarikkal, N. Fabrication of silver-decorated graphene oxide nanohybrids via pulsed laser ablation with excellent antimicrobial and optical limiting performance. *Nanomaterials* **2021**, *11*, 880. [CrossRef]
17. Rahman, S.; Mirza, S.; Sarkar, A.; Rayfield, G.W. Design and evaluation of carbon nanotube based optical power limiting materials. *J. Nanosci. Nanotechnol.* **2010**, *10*, 4805–4823. [CrossRef]

18. Sani, E.; Papi, N.; Mercatelli, L.; Barison, S.; Agresti, F.; Rossi, S.; Dell'Oro, A. Optical limiting of carbon nanohorn-based aqueous nanofluids: A systematic study. *Nanomaterials* **2020**, *10*, 2160. [CrossRef]
19. Stavrou, M.; Panacek, D.; Bakandritsos, A.; Couris, S. N-Doped Graphene and N-Doped Graphene Acid: Heteroatom Doping for Very Efficient Broad-Band Optical Limiting Performance from UV to NIR. *J. Phys. Chem. C* **2022**, *126*, 14339–14345. [CrossRef]
20. Dissanayake, D.A.S.; Cifuentes, M.P.; Humphrey, M.G. Optical limiting properties of (reduced) graphene oxide covalently functionalized by coordination complexes. *Coord. Chem. Rev.* **2018**, *375*, 489–513. [CrossRef]
21. Ma, P.C.; Siddiqui, N.A.; Marom, G.; Kim, J.K. Dispersion and functionalization of carbon nanotubes for polymer-based nanocomposites: A review. *Compos. Part A Appl. Sci. Manuf.* **2010**, *41*, 1345–1367. [CrossRef]
22. Guo, G.Y.; Chu, K.C.; Wang, D.S.; Duan, C.G. Linear and nonlinear optical properties of carbon nanotubes from first-principles calculations. *Phys. Rev. B* **2004**, *69*, 205416. [CrossRef]
23. Fashina, A.; Nyokong, T. Nonlinear optical response of tetra and mono substituted zinc phthalocyanine complexes. *J. Lumin.* **2015**, *167*, 71–79. [CrossRef]
24. Tolbin, A.Y.; Tomilova, L.G.; Zefirov, N.S. Non-symmetrically substituted phthalocyanines: Synthesis and structure modification. *Russ. Chem. Rev.* **2007**, *76*, 681–692. [CrossRef]
25. Zu, Y.; He, C.; Liu, D.; Chen, L. Synthesis of hybrid structures based on metal phthalocyanines/graphene oxide towards nonlinear optical applications. *Dyes Pigment.* **2020**, *173*, 107841. [CrossRef]
26. Kuzmina, E.A.; Dubinina, T.V.; Vasilevsky, P.N.; Saveliev, M.S.; Gerasimenko, A.Y.; Borisova, N.E.; Tomilova, L.G. Novel octabromo-substituted lanthanide (III) phthalocyanines–Prospective compounds for nonlinear optics. *Dyes Pigment.* **2021**, *185*, 108871. [CrossRef]
27. Zhao, P.; Wang, Z.; Chen, J.; Zhou, Y.; Zhang, F. Nonlinear optical and optical limiting properties of polymeric carboxyl phthalocyanine coordinated with rare earth atom. *Opt. Mater.* **2017**, *66*, 98–105. [CrossRef]
28. Erdem, M.; Korkmaz, E.; Kösoğlu, G.; Ahmetali, E.; Farajzadeh, N.; Eryürek, G.; Koçak, M.B. Nonlinear optical behavior and optical power limiting characteristics of peripheral symmetrical and non-symmetrical zinc phthalocyanines with nanosecond pulsed excitation. *Polyhedron* **2021**, *195*, 114975. [CrossRef]
29. Yadi, M.; Karimzadeh, R.; Abbasi, A. Effect of treatment by electrostatic field and 532-nm laser irradiation on optical and thermo-optical properties of graphene oxide colloids. *J. Mater. Sci.* **2017**, *52*, 4532–4542. [CrossRef]
30. Zhao, X.; Yan, X.-Q.; Ma, Q.; Yao, J.; Zhang, X.-L.; Liu, Z.-B.; Tian, J.-G. Nonlinear optical and optical limiting properties of graphene hybrids covalently functionalized by phthalocyanine. *Chem. Phys. Lett.* **2013**, *577*, 62–67. [CrossRef]
31. Sanusi, K.; Khene, S.; Nyokong, T. Enhanced optical limiting performance in phthalocyanine-quantum dot nanocomposites by free-carrier absorption mechanism. *Opt. Mater.* **2014**, *37*, 572–582. [CrossRef]
32. Nwaji, N.; Mack, J.; Nyokong, T. Enhanced nonlinear optical response of benzothiazole substituted ball-type phthalocyanines in the presence of metallic nanoparticles. *Opt. Mater.* **2018**, *82*, 93–103. [CrossRef]
33. Tolbin, A.Y.; Shestov, V.I.; Savelyev, M.S.; Gerasimenko, A.Y. Deviation from Beer's law and relationship of aggregation with the effective TPA coefficient: UV-vis studies on a series of low symmetry monophthalocyanines bearing a cyclotriphosphazene substituent. *New J. Chem.* **2023**, *47*, 1165–1173. [CrossRef]
34. Savelyev, M.S.; Gerasimenko, A.Y.; Podgaetskii, V.M.; Tereshchenko, S.A.; Selishchev, S.V.; Tolbin, A.Y. Conjugates of thermally stable phthalocyanine J-type dimers with single-walled carbon nanotubes for enhanced optical limiting applications. *Opt. Laser Technol.* **2019**, *117*, 272–279. [CrossRef]
35. Zhao, M.Q.; Liu, X.F.; Zhang, Q.; Tian, G.L.; Huang, J.Q.; Zhu, W.; Wei, F. Graphene/single-walled carbon nanotube hybrids: One-step catalytic growth and applications for high-rate Li–S batteries. *ACS Nano* **2012**, *6*, 10759–10769. [CrossRef]
36. Rozhin, A.G.; Sakakibara, Y.; Tokumoto, M.; Kataura, H.; Achiba, Y. Near-infrared nonlinear optical properties of single-wall carbon nanotubes embedded in polymer film. *Thin Solid Films* **2004**, *464*, 368–372. [CrossRef]
37. Wang, J.; Blau, W.J. Nonlinear optical and optical limiting properties of individual single-walled carbon nanotubes. *App. Phys. B* **2008**, *91*, 521–524. [CrossRef]
38. Shi, J.; Chu, H.; Li, Y.; Zhang, X.; Pan, H.; Li, D. Synthesis and nonlinear optical properties of semiconducting single-walled carbon nanotubes at 1 μm. *Nanoscale* **2019**, *11*, 7287–7292. [CrossRef]
39. Wang, A.; Du, X.; Yin, Y.; Shen, X.; Cheng, L.; Zhu, W.; Shang, D. Nonlinear optical modification of single-walled carbon nanotube by decorating with metal and metal-free porphyrins. *Diam. Relat. Mater.* **2020**, *106*, 107838. [CrossRef]
40. Tune, D.D.; Blanch, A.J.; Krupke, R.; Flavel, B.S.; Shapter, J.G. Nanotube film metallicity and its effect on the performance of carbon nanotube–silicon solar cells. *Phys. Status Solidi* **2014**, *211*, 1479–1487. [CrossRef]
41. Dresselhaus, M.S.; Dresselhaus, G.; Saito, R.; Jorio, A. Raman spectroscopy of carbon nanotubes. *Phys. Rep.* **2005**, *409*, 47–99. [CrossRef]
42. Kharlamova, M.V.; Paukov, M.; Burdanova, M.G. Nanotube Functionalization: Investigation, Methods and Demonstrated Applications. *Materials* **2022**, *15*, 5386. [CrossRef] [PubMed]
43. Vasilevsky, P.N.; Savelyev, M.S.; Tereshchenko, S.A.; Selishchev, S.V.; Gerasimenko, A.Y. Nonlinear optical properties of single-walled carbon nanotubes/water dispersed media exposed to laser radiation with nano- and femtosecond pulse durations. *Condens. Matter Interphases* **2021**, *23*, 496–506. [CrossRef] [PubMed]
44. Corletto, A.; Hosseinmardi, A.; Annamalai, P.K.; Martin, D.J.; Shapter, J.G. High-Resolution R2R-Compatible Printing of Carbon Nanotube Conductive Patterns Enabled by Cellulose Nanocrystals. *ACS Appl. Nano Mater.* **2022**, *5*, 1574–1587. [CrossRef]

45. Park, J.; Deria, P.; Olivier, J.H.; Therien, M.J. Fluence-dependent singlet exciton dynamics in length-sorted chirality-enriched single-walled carbon nanotubes. *Nano Lett.* **2014**, *14*, 504–511. [CrossRef] [PubMed]
46. Tereshchenko, S.A.; Savelyev, M.S.; Podgaetsky, V.M.; Gerasimenko, A.Y.; Selishchev, S.V. Nonlinear threshold effect in the Z-scan method of characterizing limiters for high-intensity laser light. *J. App. Phys.* **2016**, *120*, 093109. [CrossRef]
47. Lu, C.; Xuan, H.; Zhou, Y.; Xu, X.; Zhao, Q.; Bai, J. Saturable and reverse saturable absorption in molybdenum disulfide dispersion and film by defect engineering. *Photonics Res.* **2020**, *8*, 1512–1521. [CrossRef]
48. Varma, S.J.; Kumar, J.; Liu, Y.; Layne, K.; Wu, J.; Liang, C.; Nakanishi, Y.; Aliyan, A.; Yang, W.; Ajayan, P.M.; et al. 2D TiS_2 layers: A superior nonlinear optical limiting material. *Adv. Opt. Mater.* **2017**, *5*, 1700713. [CrossRef]
49. Chen, Y.; Lin, Y.; Liu, Y.; Doyle, J.; He, N.; Zhuang, X.; Bai, J.; Blau, W.J. Carbon nanotube-based functional materials for optical limiting. *J. Nanosci. Nanotechnol.* **2007**, *7*, 1268–1283. [CrossRef]
50. Wang, J.; Blau, W.J. Solvent effect on optical limiting properties of single-walled carbon nanotube dispersions. *J. Phys. Chem. C* **2008**, *112*, 2298–2303. [CrossRef]
51. Gounden, D.; Nombona, N.; Van Zyl, W.E. Recent advances in phthalocyanines for chemical sensor, non-linear optics (NLO) and energy storage applications. *Coord. Chem. Rev.* **2020**, *420*, 213359. [CrossRef]
52. Murakami, N.; Miyake, H.; Tajima, T.; Nishikawa, K.; Hirayama, R.; Takaguchi, Y. Enhanced photosensitized hydrogen production by encapsulation of ferrocenyl dyes into single-walled carbon nanotubes. *J. Am. Chem. Soc.* **2018**, *140*, 3821–3824. [CrossRef] [PubMed]
53. Chu, H.; Li, Y.; Wang, C.; Zhang, H.; Li, D. Recent investigations on nonlinear absorption properties of carbon nanotubes. *Nanophotonics* **2020**, *9*, 761–781. [CrossRef]